Recent Results on Meson Decays from A2

Patrik Adlarson for the A2 Collaboration[1,⋆]

[1] *Institut für Kernphysik, Johannes Gutenberg-Universität Mainz, D-55099 Mainz, Germany*

Abstract. Light meson decays are used to investigate topics related to fundamental aspects of particle physics. Precision measurements of meson Dalitz decays give input to theoretical evaluations of the Hadronic Light-by-Light contribution (HLbL) to the anomalous magnetic moment of the muon. The pseudoscalar η' decays allow for studies of topics like $\pi\pi$ scattering lengths, effective field theories and fundamental symmetries. The A2 collaboration, using the Crystal Ball/TAPS setup at MAMI, has recently published several high precision results on transition form factors which are related to HLbL. The value obtained for the slope parameter of the π^0 electromagnetic (e/m) transition form factor (TFF) is $a_\pi = 0.030 \pm 0.010_{tot}$. The slope parameters for the e/m TFFs of $\eta\gamma$ and $\omega\pi^0$ are $\Lambda^{-2}_{\eta\gamma} = (1.97 \pm 0.13)$ GeV^{-2} and $\Lambda^{-2}_{\omega\pi^0} = (1.99 \pm 0.22)$ GeV^{-2}, respectively. In 2014 the collaboration had a dedicated experimental campaign for the production of η' mesons. One of the main goals was to measure the dynamics of $\eta' \to \eta\pi^0\pi^0$ with high precision. An overview of the physics cases, the experimental setup and the results are given.

1 Introduction

Mesons and their properties continue to be of interest to the hadron and particles-physics communities. The electromagnetic transition form factors (TFF) are of interest for probing the precision frontier of the Standard Model (SM) but also for understanding the intrinsic properties of the hadrons themselves. In recent years, a renewed interest in the TFFs has in recent years surged as these enter as input to the theoretical calculations of the Hadronic Light-by-Light (HLbL) contributions to the anomalous magnetic moment of the muon, $(g-2)_\mu$. Also, the study of the pseudoscalar η' mesons along with its decay modes can give insight into our understanding of hadron and particles physics. Besides the η' Dalitz decay, which is related to the aforementioned $(g-2)_\mu$ determination, one can also study the decay properties and dynamics in $\eta' \to \eta\pi\pi$ and $\eta' \to \pi\pi\pi$; Pseudoscalar-Vector(PV) interactions of interest for Chiral Effective Field Theories can be studied via $\eta' \to \omega\gamma$; searches for forbidden or suppressed decays can be conducted on e.g. $\eta' \to 2\pi$, $\eta' \to 4\pi$ and $\eta' \to l^+l^-\pi^0$. In addition, photo-induced production of the η' mesons is a selective probe for studying nucleon resonances [1]. This proceeding will have, as its main focus, recent results from the A2 collaboration on meson TFF: $\pi^0 \to e^+e^-\gamma$ [2], $\eta \to e^+e^-\gamma$ and $\omega \to \pi^0e^+e^-$ [3], and the decay $\eta' \to \pi^0\pi^0\eta$. These proceedings are structured to, first, give motivations for the respective physics cases (section 2), an overview of the Crystal Ball-TAPS experimental setup at MAMI (section 3), a description of the major analysis steps (section 4), the results (section 5), and, finally a summary (section 6).

⋆e-mail: adlarson@kph.uni-mainz.de

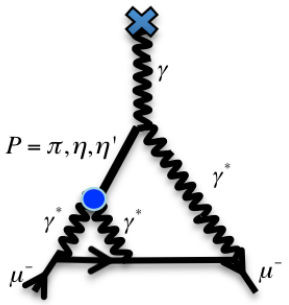

Figure 1. The Hadronic Light-by-Light contribution.

2 Motivation: a_μ and Meson TFF

Some of the most precisely known quantities in the SM are those of the anomalous magnetic moments of leptons, $a_l = (g_l - 2)/2$. Although a_e is more precisely known [4], the muon anomaly has greater sensitivity to heavier physics since the relative contribution of heavier virtual particles goes as $(m_\mu/m_e)^2 \sim 43000$ [5]. For the muon magnetic moment the most precisely measured value, which is known to the 10th decimal, comes from the E821 experiment at Brookhaven National Laboratory [6]. Comparing the E821 result to the SM calculation [7] gives a difference of $\Delta_\mu^{EXP-SM} = 28.7 \pm 8.0 \cdot 10^{-10}$, a deviation of 3.6σ. Another recent theoretical evaluation finds a deviation of 4.5σ [8]. This could be an indication of physics Beyond Standard Model, but for this to be confirmed, higher accuracy for both experiments and theory are still needed. The SM calculation to a_μ is split up into its electromagnetic (a_μ^{QED}), weak ($a_\mu^{W,Z}$) and hadronic components ($a_\mu^{hadr} = a_\mu^{HVP} + a_\mu^{HLbL}$). Although the highest contribution comes from QED, the greatest uncertainty comes from the hadronic part. New experiments are planned at Fermilab and J-PARC, with the goal to measure a_μ with a reduced uncertainty of a factor 4, $\delta a_\mu \sim 1.6 \cdot 10^{-10}$ [9, 10]. The accuracy probed by these experiments will be sensitive to mass scales of $m_\mu/(\delta a_\mu^{EXP})^{1/2} \sim 8$ TeV, thus competitive to LHC energy scales [11]. With the projected experimental accuracy, the limiting uncertainty will then be dominated by the hadronic contributions to the SM calculation of a_μ. The hadronic component of a_μ can be further sub-divided into a_μ^{HVP} and a_μ^{HLbL}, referring to the hadronic vacuum polarization (HVP) and HLbL contributions, respectively. The HVP term is dominant of the two and can be directly linked to hadronic cross-sections in e^+e^--scattering via dispersion relations. The HLbL contribution, which is the diagram shown in Fig. 1, is more difficult to estimate. Until recently, this contribution was mostly obtained from hadronic models, suffering from large and uncontrolled uncertainties [12]. Recently, however, dispersive approaches have been proposed with the goal to reduce the present day errors of the HLbL contribution. One theory group uses dispersion relations based on the analytic structure of the HLbL tensor [15], and one group based on the properties of the electromagnetic vertex function [13]. The first is also a data driven approach, which includes experimental data to evaluate the HLbL contribution in a systematical way. If the experimental data input is precise enough, this can help to constrain the dispersion relation results. Even if data are not precise enough to constrain the calculations, they can still be used to assess the predictive power of these approaches.

2.1 Motivation: Meson TFF

An important ingredient for a better understanding of the HLbL contributions comes from the study of meson TFFs [14]. The meson TFF refers to the vertex where a meson transforms to another state by emitting a virtual photon. Meson TFFs can be accessed in kinematical regions of four-momentum transfer q^2 through study of both space- and time-like processes. In Mainz, experimental activities are focused on both regions with the BESIII (space-like) and A2 (time-like) detectors [16]. Time-like TFFs can be studied in Dalitz decays and annihilation processes, while space-like TFFs are studied in photon-photon fusion processes. The TFFs with the lightest pseudo-scalar particles (π^0, η, η') are of greatest importance to the HLbL contribution as the expected importance of the contribution goes as $1/m_P^2$ [20]. The A2 collaboration can kinematically access and measure the $P = \pi^0,\ \eta,\ \eta'$ Dalitz decays, i.e. $P \to \gamma^*\gamma \to e^+e^-\gamma$, as well as the decay $\omega \to \pi^0 e^+e^-$. Quantum Electro Dynamics (QED) predicts a specific meson decay dependence on the observable $m_{ll} = \sqrt{q^2}$. As QED describes the point-like behavior of the meson decay, any deviation is attributed to the properties of the electromagnetic TFF. For the Dalitz decays, the momentum transfer range available is given by $4m_l^2 < q^2 < m_P^2$, where m_P is the mass of the pseudoscalar meson, P. This applies to the case $P \to \gamma\gamma^*$. In general, however, $A \to B\gamma^*$ has the range $m_l^2 \leq q^2 \leq (m_A - m_B)^2$. The time-like TFF is obtained by dividing the differential decay distribution with its corresponding QED contribution, e.g. $QED_{P\gamma}$. For the Dalitz decays, this is given by

$$\frac{d\Gamma(P \to l^+l^-\gamma)}{dm_{ll} \cdot \Gamma(P \to \gamma\gamma)} = |QED_{P\gamma}||F_{P\gamma}(m_{ll})|^2, \tag{1}$$

where $F_P(m_{ll})$ is the meson TFF for the Pseudoscalar Dalitz decays. For the decay $\omega \to \pi^0 e^+e^-$, the $\omega \to \pi^0\gamma^*$ TFF is

$$\frac{d\Gamma(\omega \to l^+l^-\pi^0)}{dm_{ll} \cdot \Gamma(\omega \to \gamma\pi^0)} = |QED_{\omega\pi^0}||F_{\omega\pi^0}(m_{ll})|^2. \tag{2}$$

In the Vector Meson Dominance model (VMD), the virtual photon, γ^*, couples to an intermediate virtual-vector-meson state V(e.g. ρ, ω, ϕ). This mechanism becomes more enhanced in the time-like region for decays where q is allowed to approach close to the resonance region, $q^2 = m_V^2$. An observable often used to quantify the TFF dependence is the slope parameter, a_P, which reflects the slope value extracted at $q^2 = 0$,

$$a_P \equiv \frac{F_P(m_{ll})}{dq^2}|_{q=0}. \tag{3}$$

Related to this quantity is also the effective mass Λ which, under the VMD approximation, parametrizes the TFFs in a pole approximation,

$$F_{P\gamma/\omega\pi^0}(m_{ll}) = (1 - \frac{m_{ll}^2}{\Lambda^2})^{-1},\ \Lambda^{-2} = a_P. \tag{4}$$

Due to the smallness of the momentum-transfer range for the π^0 Dalitz decay, it is parametrized as

$$F_{\pi^0\gamma}(m_{ll}) = (1 + a_\pi \frac{m_{ll}^2}{m_{\pi^0}^2}). \tag{5}$$

Experimentally, the PDG value of the slope parameter for the π^0 Dalitz decay, $a_{\pi^0} = 0.032 \pm 0.004$ [17] is dominated by the CELLO result, $a_{\pi^0} = 0.0326 \pm 0.0026_{\text{stat}} \pm 0.0026_{\text{syst}}$ [18]. It should be noted, however, that the CELLO result introduces a certain model dependence, as the slope parameter is extrapolated from the space-like region under the assumption of the validity of

VMD. Furthermore, the extrapolation is from the range of momentum transfers above 0.5 GeV^2, where the actual measurement took place, towards small momentum transfers. It is, therefore, also beneficial to have measurements of the slope parameter that does not rely on extrapolations, but are measured directly in the time-like region. Up until recently, the most accurate value of the slope parameter measured from π^0 Dalitz decay data is from the SINDRUM collaboration [19]. SINDRUM obtained $a_{\pi^0} = 0.025 \pm 0.014_{\text{stat}} \pm 0.026_{\text{syst}}$, and their result was based on the analysis of $54 \cdot 10^3$ events. More recently, and about the same time as the A2 result became available [2], the NA62 collaboration also released new results [21]. These are based on $1.05 \cdot 10^6$ Dalitz decays and the obtained value is $a_\pi = 0.0368 \pm 0.0051_{\text{stat}} \pm 0.0025_{\text{syst}}$. The most accurate theoretical descriptions of the slope-parameter are obtained from using Padé approximants [22] or dispersive theory [23], giving $a_{\pi^0} = 0.0324 \pm 0.0012_{\text{stat}} \pm 0.0019_{\text{syst}}$ and $a_\pi = 0.0307 \pm 0.0006_{\text{tot}}$, respectively.

For the η Dalitz decay, the best experimental result for the slope parameter of the Dalitz decays come from the NA60 collaboration from p–A collisions, $\Lambda_{\eta\gamma}^{-2} = (1.934 \pm 0.067_{stat} \pm 0.050_{syst})$ GeV^{-2} [24]. These are in good agreement with their first results, $\Lambda_{\eta\gamma}^{-2} = (1.95 \pm 0.17_{\text{stat}} 0.05_{\text{syst}})$ GeV^{-2} obtained in peripheral In–In data [25]. There are two previous results from the A2 collaboration at MAMI, based on $1.35 \cdot 10^3$ [26] and $2.2 \cdot 10^4$ [27] Dalitz decays. The higher-statistics result gave the value $\Lambda_\eta^{-2} = (1.95 \pm 0.15_{\text{stat}} \pm 0.10_{\text{syst}})$ GeV^{-2}. A recent theoretical prediction comes from the Jülich group, using a dispersive approach [28, 29]. In addition, there are predictions based on Padé approximants [32, 33] and using a chiral Lagrangian approach [30, 31]. For the η' Dalitz decay, the best experimental result comes from the BESIII collaboration [34].

Considering also other TFFs, much attention has been given to the time-like $\omega\pi^0$ TFF in the q-range covered by the $\omega \to \pi^0 l^+ l^+$ decay. This is because the available experimental data at high m_{ll} masses are discrepant, so far, with every available theoretical approach. The experimental data from Lepton-G [69] and NA60 [24, 25] are, however, in agreement with each other. These high mass data points, $m_{ll} > 600$ MeV, are not compatible with theoretical approaches using also model-independent assumptions. One group uses analyticity and unitarity in the framework known as the method of unitary bounds [36] and finds inconcistency between their predictions and the NA60 data. Therefore, it is of importance to obtain new experimental input that can be used for further probing the high m_{ll} mass region.

2.2 Motivation: $\eta' \to \eta\pi\pi$

As mentioned above, one of the reasons to study η' decays is due to its connection to the HLbL contribution. In general, decays of the η' meson also play an important role for our understanding of low energy Quantum Chromo Dynamics (QCD). The low-energy effective-field theory of QCD, Chiral Perturbation Theory (ChPT) is constructed from the chiral $SU(3)_L \times SU(3)_R$ symmetry in the limit of vanishing quark masses (chiral limit), with the symmetry being spontaneously broken to $SU(3)_V$ [37]. ChPT works well below m_σ and describes the interaction of the pseudoscalar mesons π, K, and η. In ChPT η' is, however, not included explicitly due to the $U(1)_A$ anomaly, which renders it massive also in the chiral limit. To include η' in a Lagrangian together with π, K, and η, one can assume that the number of color charges is large (large-N_C). Under this assumption, the $SU(3)_L \times SU(3)_R$ symmetry extends to $U(3)_L \times U(3)_R$ [38–41, 48]. How well large-N_C ChPT works is not well established and, therefore, needs to be confirmed through precision experiments. A potential drawback with large-N_C ChPT concerns the fact that it does not include resonances like ρ, a_0, σ directly as external states. They are, however, taken into account through the low energy constants. The assumption is that the

external states have higher masses compared to the center-of-mass total energy for any given process including η' and, therefore, does not need to be taken into account explicitly [41]. The validity of this assumption can, however, be questioned, and it can be argued that the resonance effects need to be considered directly. For this purpose, Resonance Chiral Theory (RChT) has been developed, where the pseudoscalars are allowed to interact with nonets of vectors, axials and scalars [42]. To test the effectiveness of the ChPT extensions, the decay $\eta' \to \eta\pi\pi$ can be used. In 2010 both frameworks were considered by using $\eta' \to \eta\pi\pi$ as a probe [41]. This decay is particularly suitable since final state interactions are mainly dominated by scalars as G-parity conservation suppresses vector contributions. In addition, as both η' and η participate in the process, the mixing properties of these two mesons can also be studied [41, 43].

There are also other motivations for studying $\eta' \to \eta\pi\pi$. In the isospin limit, the $\eta' \to \eta\pi^0\pi^0$ and $\eta' \to \eta\pi^+\pi^-$ decay amplitudes should be the same, allowing for a direct comparison of these two decay channels with theoretical predictions. Due to isospin violation, however, the virtual charge exchange reaction $\pi^+\pi^- \to \pi^0\pi^0$ gives rise to a cusp in the $m_{\pi^0\pi^0}$ spectrum visible at the mass below the $m_{\pi^+\pi^-}$ mass threshold. The effect of the cusp was first seen by NA48/2 in $K^+ \to \pi^+\pi^0\pi^0$ and it has been used to extract the S-wave $\pi\pi$ scattering length combination $a_0 - a_2$ [44–49]. For $\eta' \to \eta\pi^0\pi^0$, the cusp effect and its size has been predicted within the framework of the non-relativistic effective-field theory to be about 6%, compared to phase space [50]. Previously, also the $\eta' \to \eta\pi\pi$ Dalitz plot parameters were estimated within the framework of U(3) chiral effective-field theory in combination with a relativistic coupled-channels approach [51–53].

The first experimental data on the neutral decay mode, $\eta' \to \eta\pi^0\pi^0$, was taken by the GAMS-2000 spectrometer at the IHEP accelerator U-70 with $5.4 \cdot 10^3$ measured decays [54]. A higher statistics sample was made a few years later as the upgraded GAMS-2000 spectrometer, GAMS-4π, in 2009 measured $1.5 \cdot 10^4$ events [55]. The corresponding decay with charged pions $\eta' \to \eta\pi^+\pi^-$ has been measured with higher statistics by the VES [56] and BESIII [57] collaborations. The highest-statistics results come from the BESIII collaboration measuring $\sim 43.8 \cdot 10^3$ decays. An updated result from BESIII is foreseen in the near future with even higher statistics in the final event sample.

To describe the matrix element for the $\eta' \to \eta\pi_1\pi_2$ decay the Dalitz plot is used. Three body decays can be expressed in terms of the variables X and Y, defined as

$$X = \frac{\sqrt{3}}{Q}(T_{\pi_1} - T_{\pi_2}), \quad Y = \frac{T_\eta}{Q}(\frac{m_\eta}{m_\pi} + 2) - 1 \, . \tag{6}$$

The observables T_{π_1}, T_{π_2} denote the kinetic energies of the two final-state pions and T_η denotes the kinetic energy of η. All kinetic energies are calculated in the η' rest frame. The sum of the kinetic energies are given by Q, $Q = T_\eta + T_{\pi_1} + T_{\pi_2} = m_{\eta'} - m_\eta - 2m_\pi$. The Dalitz plot is expanded around $X = Y = 0$ and a polynomial is used to describe the matrix element. The polynomial parametrization used in the most recent measurements [55–57] is given in the form

$$|M|^2 \sim 1 + aY + bY^2 + cX + dX^2, \tag{7}$$

where a, b, c and d are Dalitz plot parameters. All Dalitz plot parameters of odd-powered X are expected to be consistent with 0 for symmetry reasons. For $\eta' \to \pi^0\pi^0\eta$ this is due to Bose-Einstein symmetry of the wave function, and for $\eta' \to \pi^+\pi^-\eta$ as a consequence of charge-conjugation symmetry. For the $\eta' \to \pi^0\pi^0\eta$, it is not possible to distinguish the two neutral pions from each other. By definition, $T_{\pi_1} > T_{\pi_2}$, which means that X is always greater or equal to 0. Therefore, any odd-powered dependence on X, e.g. the cX term, makes no sense in the neutral channel. Some

Experiment $\eta' \to \pi^0\pi^0\eta$	***a***	***b***	***d***
GAMS4π [55]	-0.067(16)(4)	-0.064(29)(5)	-0.067(20)(3)
Experiment $\eta' \to \pi^+\pi^-\eta$			
VES [56]	-0.127(16)(8)	-0.106(28)(14)	-0.082(17)(8)
BESIII [57]	-0.047(11)(3)	-0.069(19)(9)	-0.073(12)(3)
Theory $\eta' \to \pi\pi\eta$			
Large-Nc* [41]	-0.098(48)	-0.050(1)	-0.092(8)
RChT* [41]	-0.098(48)	-0.033(1)	-0.072(8)
U(3) Ch.EFT ($\eta' \to \pi^+\pi^-\eta/\eta' \to \pi^0\pi^0\eta$) [53]	-0.123/-0.109	-0.104/-0.087	-0.047/-0.036

Table 1. Dalitz plot-parameter results for $\eta' \to \pi\pi\eta$ measurements and calculations with errors given in the parentheses. For the experimental data, the first and second parentheses denote the statistical and systematical errors, respectively. *In ref [41] parameter values of $eY \cdot X^2$ and $f \cdot X^4$ are given. For Large-Nc, $e = 0.003(2)$ and $f = 0.002(1)$ while, for RChT, $e = -0.009(2)$ and $f = 0.001(1)$.

recent experimental determinations and theoretical estimates of the Dalitz plot parameters are given in Table 1. There is an ambiguity in the Dalitz plot parameters for the charged Dalitz plot parameters a and b when comparing the VES [56] and BESIII [57] result. Given the connection between the charged and neutral decays and the predicted cusp effect, a new high precision measurement would, therefore, provide valuable input into better understanding QCD dynamics.

3 Experimental Setup

The electron accelerator MAMI (Mainz Microtron) [58, 59] at the Institute for Nuclear Physics of the University of Mainz consists of a cascade of several accelerators, which allows the production of an unpolarized or polarized continuous wave electron beam with nominal energies up to 1.604 GeV. The photon beam were produced, for the experiments described here, when the electron beam interacted with a thin 10-μm Cu radiator producing bremsstrahlung electrons and photons. To reduce the width of the beam, the beam photons are collimated by a Pb collimator before entering the target region. The Pseudoscalar (P= π^0, η, η') and Vector (V=ω) particles are produced when the bremsstrahlung photons impinge on a 5 or 10 cm long Liquid Hydrogen target (LH_2), $\gamma p \to P/Vp$. The corresponding postbremsstrahlung electrons are detected in a tagger, providing the measurement of the energy, E_γ, of photons incident to the target. There are two different taggers, for energies covering ~0.08-1.5 GeV the Glasgow-Mainz tagger is used [60–62]. For photon beam energies needed to produce η' a special tagging device was built, the so-called end-point tagging spectrometer (EPT) [63] with the purpose of tagging postbremsstrahlung electrons with very low energy. The final state $e^\pm$- and γ-particles from the meson decays are measured by using the Crystal Ball (CB) [64] and TAPS [65, 66], being the central and forward calorimeters, respectively. The experimental setup is shown in figure 2. The CB detector consists of 672 NaI(Tl) crystals which are formed into a sphere. The sphere encapsulates the LH_2 target and covers 93% of 4π. Also covering the target is the Particle Identification Detector (PID), made of 24 scintillator bars. Its main purpose is to separate charged from neutral particles. The PID becomes important for the TFF analyses where one needs to suppress charge conversion events from e.g. $P \to \gamma\gamma$ events. The TAPS detector is installed 1.5 m downstream and consists of 384 hexagonal BaF_2 crystals. In the η' experiment, 18 of the BaF2 crystals closest to the beamline were replaced with 72 $PbWO_4$ crystals. This enabled running with a

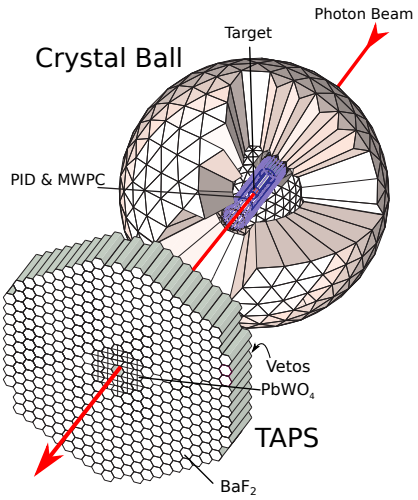

Figure 2. The Crystal Ball and TAPS experimental setup, indicating the direction of the photon beam as the red arrow. For the η' production run the 18 innermost TAPS BaF_2 crystals were replaced with 72 $PbWO_4$ crystals.

higher MAMI electron current, without decreasing the TAPS efficiency due to the higher count rate. The experimental trigger was set to exceed a given energy sum collected in the CB.

The results presented here are from several different run periods between the years 2007-2014, spanning different photon beam energy ranges. For the π^0 Dalitz decay two beam times were used: the first by tagging the bremsstrahlung electrons in the E_γ range 140-800 MeV and the second in the tagged E_γ range 220-1450 MeV. The η Dalitz and $\omega \to \pi^0 e^+ e^-$ decays were collected and analyzed using the two same runs. In the first run, the energies of the incident photons were analyzed up to 1402 MeV and in the second run up to 1448 MeV. The EPT run aimed at producing η' with the maximum electron-beam energy of MAMI, 1.604 GeV, which allowed to tag the E_γ range 1426-1577 MeV.

4 Analysis

4.1 $\pi^0 \to e^+e^-\gamma$

The π^0 Dalitz decay was searched for in events containing 3 and 4 reconstructed clusters. For 3-cluster events it was assumed that the missing cluster is the proton, which can happen when the proton energy is low and fails to escape the target region. For the selection of the final event sample and determination of the kinematics, kinematic fit was used [67]. For details of the kinematic fit, its parametrizations and resolutions, the interested reader is referred to [68]. Kinematic fit was used both to select the signal and rejecting the main background contribution coming from $\pi^0 \to \gamma\gamma$ events. For signal selection, only events with a Confidence Level (CL)>1% for the hypothesis $\gamma p \to p3\gamma$ were kept for further analysis. The electromagnetic showers for electrons/positrons are similar to γ, such that $\gamma p \to p3\gamma$ can be tested to identify $\gamma p \to pe^+e^-\gamma$. Kinematic-fit was also used as a veto rejecting events which fulfilled the hypothesis $\gamma p \to p\pi^0 \to p\gamma\gamma$ with CL>10^{-5}. The lepton pairs

were distinguished from photons by selecting CB clusters which also had matching hits in the PID. To reduce background from conversion events of $\pi^0 \to \gamma\gamma$, an additional requirement was also that two different PID elements were fired. Both the signal and background contributions were simulated in Monte Carlo (MC) to reflect their actual behavior in the experiment, both in terms of the production cross sections and for the decay dynamics. The final event sample was split up into 18 bins with respect to $m(e^+e^-)$ in the range 15-120 MeV. In each bin, the actual Dalitz-decay-signal contents was found by fitting a polynomial on the remaining, but small, non-resonant background together with a Gaussian giving $\sim 4.0 \cdot 10^5$ π^0 Dalitz decays.

4.2 $\eta \to e^+e^-\gamma$ and $\omega \to e^+e^-\pi^0$

Similarly to the π^0 Dalitz decay, $\eta \to e^+e^-\gamma$ and $\omega \to e^+e^-\pi^0$ were also selected first by identifying the number of final state clusters. For the η Dalitz decay both 3- and 4-cluster events were selected, whereas, for the ω decay, only 5-cluster events was selected for further analysis. 4-cluster events were neglected in the ω analysis as the proton information missing for such events resulted in much larger background contributions. The kinematic fit was used to identify the signal channels as well as suppressing background. For the ω channel, the hypotheses $\gamma p \to 4\gamma p$ and $\gamma p \to \pi^0\gamma\gamma \to 4\gamma p$ were tested, while, for the η Dalitz decay the hypothesis $\gamma p \to 3\gamma p$ was tested. The main background for the η Dalitz decay with three cluster events comes from $\pi^0 \to \gamma\gamma$ and $\eta \to \gamma\gamma$. To reject these events, the kinematic-fit hypotheses tested also $\gamma p \to \pi^0 p$ and $\gamma p \to \eta p$. If the CL was found to be greater than 10^{-5} for the two latter hypotheses, these events were rejected. After kinematic-fit selection, the lepton pairs were identified by selecting clusters with matching hits in the PID. For the η Dalitz decay, the only serious background candidate was $\eta \to \gamma\gamma$ with one photon undergoing conversion in the material between the production vertex and the calorimeter material. For the ω, there are three major sources of background: $\gamma p \to \pi^0\pi^0 p$, $\gamma p \to \pi^0\eta p$ and $\omega \to \pi^+\pi^-\pi^0$. Suppressing the first two background channels required analysis of energy losses, dE/dx, in the PID elements, while to suppress $\omega \to \pi^+\pi^-\pi^0$, cuts on the kinematic-fit CL, vertex cuts and using the fact that nuclear-interaction and electromagnetic showers interact differently with the CB crystals were needed. After final event selection for the η Dalitz decay and $\omega \to \pi^0 e^+e^-$, the sample was split up into bins with respect to $m(e^+e^-)$ and for each bin, the signal content was estimated by fitting a polynomial and Gaussian to the experimental data. In the remaining final event sample, $\sim 5.4 \cdot 10^4$ η Dalitz decays and $\sim 1.1 \cdot 10^3$ $\omega \to \pi^0 e^+e^-$ decays were obtained.

4.3 $\eta' \to \eta\pi^0\pi^0$

The process $\gamma p \to \eta' p \to \pi^0\pi^0\eta p \to 6\gamma p$ was searched for in events reconstructed with 7 clusters detected in both CB and TAPS, assuming that one of the clusters was due to the recoil proton. In the beam energy range of when producing η', most of the recoil protons were produced within the polar angle covered by TAPS. Study of background reactions with MC simulations showed that the process $\gamma p \to 3\pi^0 p \to 6\gamma p$ can mimic $\gamma p \to \pi^0\pi^0\eta p \to 6\gamma p$ if the invariant mass is greater than ~ 820 MeV. This can happen when invariant masses of the three $\gamma\gamma$ pairs, $m(\gamma\gamma)$, are found close to two masses of π^0 and a mass of η. Similarly, the process $\gamma p \to \pi^0\eta p \to 4\pi^0 p \to 8\gamma p$ can mimic the signal channel when two of the eight final-state photons are not detected. Suppression of the $\gamma p \to 3\pi^0 p \to 6\gamma p$ background was done by testing the corresponding kinematical-fit hypothesis and applying a CL cut. For the final event sample, the requirement on the signal channel was CL>0.02. It was also required that the hypothesis $\gamma p \to 3\pi^0 p \to 6\gamma p$ had to have a CL<0.08. The sample of remaining events is shown in the left frame of Fig. 3. It is seen that there is still a non-peaking background distribution to be accounted for in the final event sample. To estimate the signal content in the Dalitz plot, the data

were, first, distributed into bins corresponding to different regions in X and Y of the Dalitz plot. Then the data were fitted with a polynomial of order 4 together with the MC η' signal line shape. The MC η' signal line shape came from a large statistics sample obtained under the same analysis condition as the experimental distribution. The estimated number of $\eta' \to \eta\pi^0\pi^0$ decays in the final event sample is $\sim 1.4 \cdot 10^5$.

5 Results

5.1 Meson TFF

The total number of π^0/η Dalitz decays and $\omega \to \pi^0 e^+ e^-$ was corrected for the efficiency in each bin of $m(e^+e^-)$. To obtain the transition form factors $|F_{\pi^0\gamma}|$, $|F_{\eta\gamma}|$ and $|F_{\omega\pi^0}|$, the number of events in each bin was divided by the corresponding QED contributions and decay widths, $\Gamma(P \to \gamma\gamma)$, $\Gamma(\omega \to \pi^0\gamma)$. The form factor $|F_{\pi^0\gamma}|^2$, shown as a function of $m(l^+l^-)$ for the π^0 Dalitz decay, is seen in Fig. 4. Similarly, the $|F_{\eta\gamma}|^2$ and $|F_{\omega\pi^0}|^2$ are shown in Figs. 5 and 6, respectively. The statistical uncertainty in an individual bin of $|F_{P\gamma}|^2$ and $|F_{\omega\pi^0}|^2$ was given by the uncertainty in estimating the number of decays as determined by the Gaussian and polynomial fitting. The systematic uncertainties were estimated for each individual $m(e^+e^-)$ bin by repeating its fitting procedure several times after refilling the experimental $m(e^+e^-\gamma)/m(e^+e^-\pi^0)$ spectra under different selection criteria used in the analysis, e.g. cuts on the kinematical fit CL, different cuts on PID, dE/dx, cluster radius and z-vertex position. By testing several different fits, this showed the concistency of the results. The average of the results for all fits made for one bin was used to obtain the final form factor values. The systematic uncertainties were taken as the root mean square of all the results from each bin.

By fitting Eqs. (4) and (5) to the form factor data points, the pole approximation and its slope parameter were obtained. For the π^0 Dalitz decay, this gives $a_\pi = 0.030 \pm 0.010_{\text{tot}}$, which is in good agreement with the PDG value [17], the recent NA62 result [21] and theoretical estimates [22, 23]. For the data points of the η Dalitz decay, the fit with the pole approximation, (Eq. 4), gives the fitted value $\Lambda_\eta^{-2} = (1.97 \pm 0.13)$ GeV^{-2}, which is in agreement with the latest NA60 result [24] and theoretical calculations [29, 30, 32, 33]. The fit value obtained for $|F_{\omega\pi^0}|$, $\Lambda_{\omega\pi^0}^{-2} = (1.99 \pm 0.21_{\text{tot}})$ GeV^{-2}, is a bit lower compared to previous measurements from NA60, $\Lambda_{\omega\pi^0}^{-2} = (2.223 \pm 0.026_{\text{stat}} \pm 0.037_{\text{syst}})$ GeV^{-2} [24]. The new result from the A2 collaboration is in better agreement with theoretical calculations, compared to the data from other experiments. A firm conclusion may not be drawn presently as the accuracy of the present data points at large $m(e^+e^-)$ masses is not sufficient for it. More high-statistics measurements of the $\omega \to \pi^0 e^+ e^-$ decay, especially at large $m(e^+e^-)$ masses, are needed to solve the problem of the inconsistency remaining between the calculations and the experimental data.

5.2 $\eta' \to \eta\pi^0\pi^0$

The Dalitz plot for the final event sample is shown in the right frame of Fig. 3 for the bin width ΔX=ΔY =0.1. The fit function minimized in MINUIT [75] is

$$\chi^2 = \sum_{i=1}^{bins} \left(\frac{N_i - \sum_{i=1}^{nbins} \epsilon_i \cdot f(X_i, Yi)}{\sigma_i} \right)^2 \tag{8}$$

where N_i is the experimentally reconstructed number of events in bin i and ϵ_i is the efficiency for the same bin and $f(X_i, Y_i)$ is the fitting function given in Eq. 6. The bins are represented one-dimensionally and are calculated such that a bin number specifies a rectangular area in the Dalitz

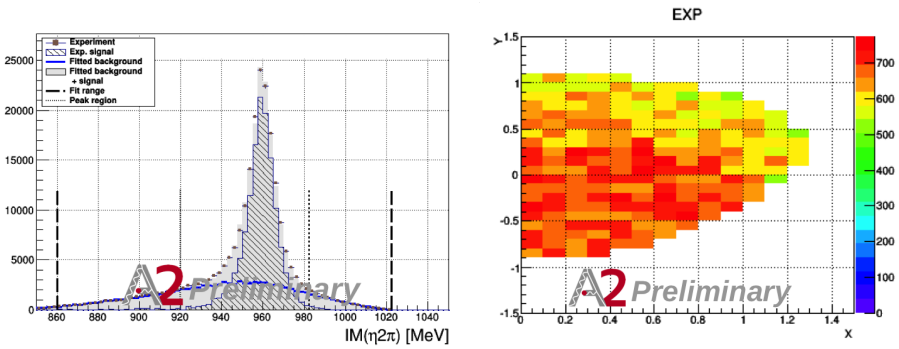

Figure 3. (left) The final event sample for the decay $\eta' \to \eta\pi^0\pi^0$. (right) The preliminary Dalitz plot with a bin width of 0.1.

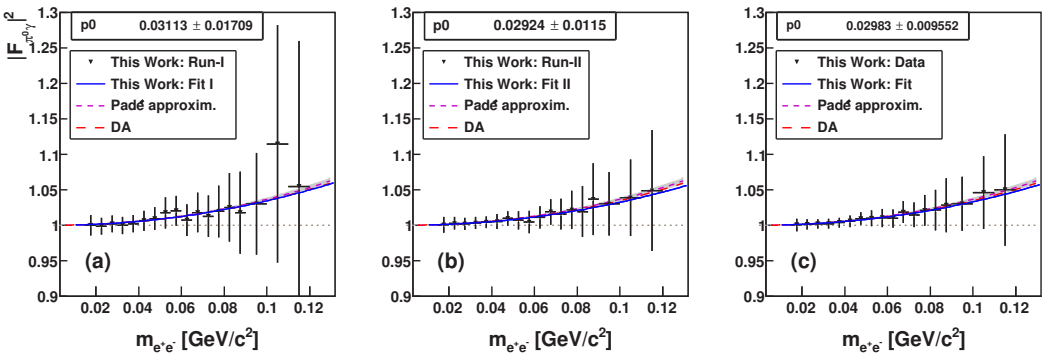

Figure 4. $|F_{\pi^0\gamma}|^2$ results with total uncertainties (black filled triangles) from two different run sets: Run 1 (a), Run 2 (b). The combined result is shown in (c). The fitted values to the points are shown by blue lines, with $p0$ being the slope parameter a_π. Comparison to calculations with Padé approximants [22] is seen as the short-dashed magenta line with a gray error band and to the dispersive analysis (DA) [23] shown as the red, long-dashed line. The error band for the latter analysis is by a factor of four narrower, compared [22], and is omitted.

plot region. The efficiency, ϵ_i, is obtained from a high statistics MC sample of $9 \cdot 10^6$ signal events. The preliminary values for the Dalitz-plot parameters are given in table 2. The preliminary results are in good agreement with the GAMS4π results, but have a better statistical accuracy. Investigation of systematic effects as well as a detailed study of the cusp region are in progress.

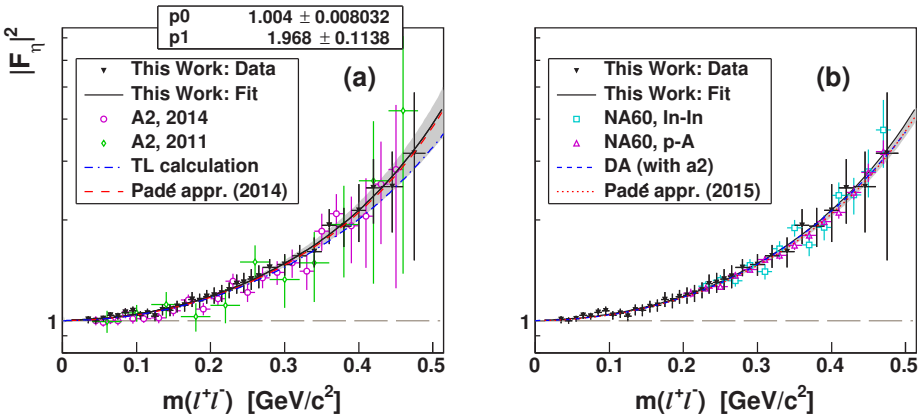

Figure 5. $|F_{\eta\gamma}(m_{e^+e^-})|^2$ results (black filled triangles) fitted with the pole approximation (black solid line). $p0$ and $p1$ denotes the normalization and slope parameter Λ^{-2}, respectively. The former results from the A2 Collaboration [27] (open magenta circles) and [26] (open green diamonds) are shown in panel (a). The results of NA60 from peripheral In–In data [25] and p–A collisions [24] are seen in (b). The calculation from Ref. [30] is seen in (a) as a blue dash-dotted line. The recent dispersive approach [29] is shown in (b) by a blue dashed line. The calculations with Padé approximants are shown in (a) for a previous solution [32] (red dashed line with an error band) and in (b) for the latest solution [33] (red dotted line with an error band).

Result	***a***	***b***	***d***	χ^2**/dof**
A2 Preliminary	-0.075(8)	-0.069(13)	-0.054(8)	247.6/195 = 1.27

Table 2. *Preliminary results of A2 for the Dalitz-plot parameters of $\eta' \to \eta\pi^0\pi^0$. Uncertainties (inside the parentheses) are statistical.*

6 Summary

In these proceedings, three new results from the A2 collaboration were presented for the TFFs $|F_{\pi^0\gamma}|$, $|F_{\eta\gamma}|$ and $|F_{\omega\pi^0}|$. The results were obtained by analyzing the decays $\pi^0 \to e^+e^-\gamma$, $\eta \to e^+e^-\gamma$ and $\omega \to \pi^0e^+e^-$. The slope parameters for the e/m TFF of $\pi^0\gamma$, $\eta\gamma$ and $\omega\pi^0$ are $a_\pi = 0.030 \pm 0.010$, $\Lambda^{-2}_{\eta\gamma} = (1.97 \pm 0.13)$ GeV^{-2} and $\Lambda^{-2}_{\omega\pi^0} = (1.99 \pm 0.22)$ GeV^{-2}, respectively. While the results for the π^0 and η Dalitz decays are in agreement with other experimental results and theoretical calculations, the $\omega \to \pi^0e^+e^-$ result from A2 are in a better agreement with theoretical calculations, compared to the available experimental data. However, because of limited experimental statistics, no firm conclusion can be drawn to rule out the previous results. For the $\eta' \to \eta\pi^0\pi^0$ the preliminary results of the Dalitz-plot parameters are presented and the systematic effect are currently under investigation. In addition to the analysis of $\eta' \to \eta\pi^0\pi^0$ analyses of $\eta' \to e^+e^-\gamma$, $\eta' \to \omega\gamma$ and $\omega \to \eta\gamma$ with the A2 data are in progress as well.

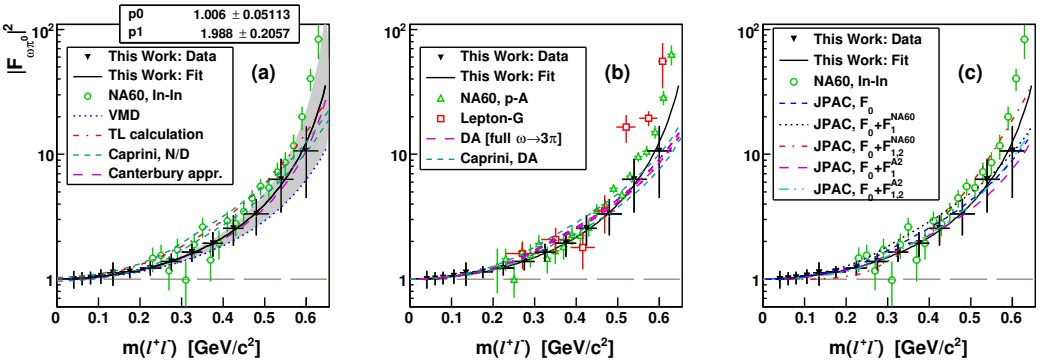

Figure 6. $|F_{\omega\pi^0}(m_{e^+e^-})|^2$ results (black filled triangles) fitted with the pole approximation (black solid line). $p0$ and $p1$ denotes the normalization and slope parameter Λ^{-2}, respectively. Earlier experimental results are Lepton-G [69] (open red squares in (b)); NA60 in peripheral In–In data [25] (open green circles in (a) and (c)); NA60 in p–A collisions [24] (open green triangles in (b)). There are several theoretical calculations: The VMD prediction (blue dashed line in (a)); calculation from Refs. [30, 31] is shown by a red dash-dotted line in (a); dispersive analysis calculation by the Bonn group [70] (shown by error-band borders, magenta dashed lines in (b)); upper and lower bounds by Caprini [71] (cyan dashed lines) for two cases of the discontinuity calculated with the partial-wave amplitude $f_1(t)$ based on the improved N/D model [72] (a), and from [70] (b); calculation based on a model-independent method using Canterbury approximants [73] (magenta long-dashed line with gray error band); basic calculation from JPAC [74] (blue dashed line in (c)) and inclusion of higher order terms of the inelastic contributions in the $\omega\pi^0$ TFF by a fit to the NA60 In–In data, for the solutions with adding one (black dotted line, in (c)) and two (red dash-dotted line in (c)) terms; similar effect from including higher order terms by fitting them to present $|F_{\omega\pi^0}(m_{\ell^+\ell^-})|^2$ results shown for solutions with one (magenta long-dashed line in (c)) and two terms (cyan dash-double-dotted line in (c)).

References

[1] V. L. Kashevarov *et al.* **(A2 Collaboration at MAMI)**, arXiv:1701.04809 [nucl-ex].
[2] P. Adlarson *et al.* **(A2 Collaboration at MAMI)**, arXiv:1611.04739 [hep-ex].
[3] P. Adlarson *et al.* **(A2 Collaboration at MAMI)**, arXiv:1609.04503 [hep-ex].
[4] D. Hanneke, S. Fogwell and G. Gabrielse Phys. Rev. Lett. **100**, 120801 (2008).
[5] T. Blum, A. Denig, I. Logashenko, E. de Rafael, B. L. Roberts, T. Teubner, G. Venanzoni, arXiv:1311.2198 [hep-ph].
[6] G. W. Bennett, *et al.* **(The g-2 Collaboration)**, Phys. Rev. D**73**, 072003 (2006).
[7] M. Davier, A. Hoecker, B. Malaescu, Z. Zhang. Eur. Phys. J. C**71**, 1515 (2011).
[8] M. Benayoun, P. David, L. DelBuono, F. Jegerlehner, Eur. Phys. J. C 75, 613 (2015).
[9] J. Grange *et al.* **(Muon g-2 Collaboration)**, FERMILAB-FN-0992-E, FERMILAB- DESIGN-2014-02.
[10] T. Mibe **(J-PARC g-2 Collaboration)**, Chinese Physics C **34**, 745 (2010).
[11] A. Czarnecki and W.J. Marciano, Phys. Rev. **D** 64, 013014 (2001).
[12] A. Nyffeler, Phys.Rev. D**94** no.5, 053006 (2016).

[13] V. Pauk, M. Vanderhaeghen, Phys. Rev. D 90, 113012 (2014).
[14] L. G. Landsberg, Phys. Rep. **128**, 301 (1985).
[15] G. Colangelo, M. Hoferichter, M. Procura, JHEP 1409, **091** (2014); G. Colangelo, M. Hoferichter, B. Kubis, M. Procura, P. Stoffer, Phys. Lett. B **738**, 6 (2014); G. Colangelo, M. Hoferichter, M. Procura and P. Stoffer JHEP **1509**, 074 (2015); see B. Kubis, S. Leupold, M. Procura, these proceedings.
[16] See C. Redmer, these proceedings.
[17] C. Patrignani *et al.* **(Particle Data Group)**, Chin. Phys. C **40**, 100001 (2016).
[18] H. J. Behrend *et al.* **CELLO Collaboration**, Z. Phys. C **49** (1991) 401 (1991).
[19] R. Meijer Drees *et al.*, **SINDRUM Collaboration**, Phys. Rev. D **45**, 1439 (1992).
[20] E. Czerwinski, S. Eidelman, C. Hanhart, B. Kubis, A. Kupść, S. Leupold, P. Moskal, S. Schadmand, arXiv:1207.6556 [hep-ph].
[21] C. Lazzeroni *et al.* **(NA62 Collaboration)**, arXiv:1612.08162 [hep-ex].
[22] P. Masjuan, Phys.Rev. D **86**, 094021 (2012).
[23] M. Hoferichter. B. Kubis, S. Leupold, F. Niecknig, S.P. Schneider, Eur. Phys. J. C **74**, 3180 (2014); See S. Leupold, these proceedings.
[24] R. Arnaldi *et al.*, Phys. Lett. B **757**, 47 (2016).
[25] R. Arnaldi *et al.*, Phys. Lett. B **677**, 260 (2009).
[26] H. Berghäuser *et al.*, Phys. Lett. B **701**, 562 (2011).
[27] P. Aguar-Bartolome *et al.* Phys. Rev. C **89**, 044608 (2014).
[28] C. Hanhart, A. Kupść, U.-G. Meißner, F. Stollenwerk, and A. Wirzba, Eur. Phys. J. C **73**, 2668 (2013); *ibid.* **75**, 242 (2015).
[29] C. W. Xiao, T. Dato, C. Hanhart, B. Kubis, U.-G. Meißner, A. Wirzba, arXiv:1509.02194 [hep-ph].
[30] C. Terschlüsen, Diploma Thesis, University of Gießen, 2010.
[31] C. Terschlüsen, S. Leupold, and M. F. M. Lutz, Eur. Phys. J. A **48**, 190 (2012).
[32] R. Escribano, P. Masjuan, and P. Sanchez-Puertas, Phys. Rev. D **89**, 034014 (2014).
[33] R. Escribano, P. Masjuan, and P. Sanchez-Puertas, Eur. Phys. J. C **75**, 414 (2015).
[34] M. Ablikim *et al.* **BESIII collaboration**, Phys. Rev. D 92, 012001 (2015).
[35] R. I. Dzhelyadin *et al.*, Phys. Lett. B **102**, 296 (1981).
[36] B. Ananthanarayan, I. Caprini, and B. Kubis, Eur. Phys. J. C **74**, 3209 (2014).
[37] J. Gasser, H. Leutwyler, Nucl. Phys., B **250**, 465 (1985).
[38] G. ´t Hooft, Nucl. Phys., B **72**, 461 (1974).
[39] E. Witten, Nucl. Phys., B **156**, 269 (1979).
[40] R. Kaiser, H. Leutwyler, Eur. Phys. J., C **17**, 623 (2000).
[41] R. Escribano, P. Masjuan, J. J. Sanz- Cillero. JHEP, **05**, 094 (2011).
[42] G. Ecker, J. Gasser, A. Pich, E. de Rafael, Nucl. Phys. B **321**, 311 (1989).
[43] P. Bickert, P. Masjuan, S. Scherer, arXiv:1612.05473.
[44] J. R. Batley et al. Phys. Lett., B**633**, 173 (2006).
[45] N Cabibbo. Phys. Rev. Lett., **93** 121801 (2004).
[46] N Cabibbo, G. Isidori, JHEP, **03** 021 (2005).
[47] G. Colangelo, J. Gasser, B. Kubis, A. Rusetsky, Phys. Lett. B **638**, 187, (2006).
[48] E. Gamiz, J. Prades, I. Scimemi, Eur. Phys. J., C **50**, 405 (2007).
[49] M. Bissegger, A. Fuhrer, J. Gasser, B. Kubis, A. Rusetsky, Nucl. Phys., B **806**, 178 (2009).

[50] B Kubis, S P. Schneider, Eur. Phys. J., C**62**, 511 (2009).
[51] N. Beisert, B. Borasoy, Nucl. Phys. A, **716** 186 (2003).
[52] B. Borasoy, R. Nissler, Eur. Phys. J. A, **26** 383 (2005).
[53] B. Borasoy, Ulf-G. Meissner, R. Nissler, Phys. Lett., B **643**, 41 (2006).
[54] D. Alde *et al.* **(LAPP collaboration)**, Phys. Lett., B **177** 115 (1986), [Yad. Fiz.45,117(1987)].
[55] A. M. Blik *et al.* **(GAMS4π collaboration)**, Phys. Atom. Nucl. **72** 231 (2009), [Yad. Fiz.72,258(2009)].
[56] V. Dorofeev *et al.* **(VES Collaboration)**, Phys. Lett., B **651** 22 (2007).
[57] M. Ablikim *et al.* **(BESIII Collaboration)**, Phys. Rev. D **83**, 012003 (2011).
[58] H. Herminghaus *et al.*, IEEE Trans. Nucl. Sci. **30**, 3274 (1983).
[59] K.-H. Kaiser *et al.*, Nucl. Instrum. Methods Phys. Res. A **593**, 159 (2008).
[60] I. Anthony *et al.*, Nucl. Instrum. Methods Phys. Res. A **301**, 230 (1991).
[61] S. J. Hall *et al.*, Nucl. Instrum. Methods Phys. Res. A **368**, 698 (1996).
[62] J. C. McGeorge *et al.*, Eur. Phys. J. A **37**, 129 (2008).
[63] P. Adlarson *et al.*, Phys. Rev. C 92, 024617 (2015).
[64] A. Starostin *et al.*, Phys. Rev. C **64**, 055205 (2001).
[65] R. Novotny, IEEE Trans. Nucl. Sci. **38**, 379 (1991).
[66] A. R. Gabler *et al.*, Nucl. Instrum. Methods Phys. Res. A **346**, 168 (1994).
[67] V. Blobel E. Lohrmann. Statistische Methoden der Datenanalyse. Teubner Studienbücher, Teubner, e-book http://www.desy.de/ blobel/eBuch.pdf, 1998.
[68] S. Prakhov *et al.*, Phys. Rev. C **79**, 035204 (2009).
[69] R. I. Dzhelyadin *et al.*, Phys. Lett. B **102**, 296 (1981).
[70] S. P. Schneider, B. Kubis, and F. Niecknig, Phys. Rev. D **86**, 054013 (2012).
[71] I. Caprini, Phys. Rev. D **92**, 014014 (2015).
[72] G. Köpp, Phys. Rev. D **10**, 932 (1974).
[73] P. Masjuan, private communication with Sergey Prakhov, 2016.
[74] I. V. Danilkin, C. Fernández-Ramírez, P. Guo, V. Mathieu, D. Schott, M. Shi, and A. P. Szczepaniak, Phys. Rev. D **91**, 094029 (2015).
[75] F. James, MINUIT Function Minimization and Error Analysis: Reference Manual Version 94.1, 1994.